

Precision Studies of the Higgs Golden Channel $H \rightarrow ZZ^* \rightarrow 4\ell$. Part I. Kinematic discriminants from leading order matrix elements

Paul Avery,^a Dimitri Bourilkov,^a Mingshui Chen,^a Tongguang Cheng,^a Alexey Drozdetskiy,^a James S. Gainer,^{a,1} Andrey Korytov,^a Konstantin T. Matchev,^a Predrag Milenovic,^a Guenakh Mitselmakher,^a Myeonghun Park,^b Aurelijus Rinkevicius,^a and Matthew Snowball^a

^a*Physics Department, University of Florida, Gainesville, FL 32611, USA.*

^b*CERN Physics Department, Theory Division, CH-1211 Geneva 23, Switzerland.*

ABSTRACT: The importance of the $H \rightarrow ZZ^* \rightarrow 4\ell$ “golden” channel has recently been proven by its major role in the discovery, by the ATLAS and CMS collaborations, of an apparently Higgs-like resonance with mass near 125 GeV. Much previous phenomenological work on this channel focuses on its use in determining the spin and CP properties of a purported Higgs boson. Significantly less attention has been paid to the logically prior question of distinguishing signal from background events in this channel, which is especially important for a 125 GeV Higgs boson. We show the advantages of using a multivariate analysis, such as the Matrix Element Method (MEM) that will be discussed here, in separating the Higgs signal from the irreducible Standard Model background. We discuss a number of issues that may arise in the use of the MEM and compare existing leading order MEM-based approaches and software. We also provide a code to calculate a kinematic discriminant, KD , based on the full leading order matrix elements, which would aid experimentalists and phenomenologists in their continuing studies of the “golden” Higgs channel. The code contains the most general parameterization of the couplings of a spin zero resonance and can be used for studies of its properties as well.

¹Corresponding author: gainer@phys.ufl.edu.

Contents

1	Introduction	1
2	Preliminaries	3
2.1	The matrix element method and its kinematic discriminant KD	4
2.2	ROC curves	6
2.3	Event generation	6
2.4	Comparison with single variable analyses	7
2.5	Overview of available tools for calculating KD	7
3	KD from MADGRAPH	9
4	KD from CALCHEP	9
5	KD from MCFM	10
6	Performance summary	12
7	Improvement by including information about the initial state	13
8	Summary and outlook	15
A	Notation and conventions	15
B	The Matrix Element (ME) Kinematic Discriminant (KD) Producer	16
B.1	Description of the code	16
B.2	User instructions	18
B.2.1	Requirements	18
B.2.2	Setup of the ME KD code	19
B.2.3	Run the ME KD producer	19
B.2.4	Output from the ME KD producer	19
B.2.5	Comparison of user ME KD results	19

1 Introduction

The CERN LHC collaborations recently reported the observation of a new bosonic particle with mass $M \sim 125$ GeV [1, 2]. The production rates in the main discovery channels are consistent with the expectations for the Higgs boson, H , of the Standard Model (SM). The relatively large amount of new data collected by the LHC experiments in 2012 makes possible the first detailed studies of the properties of this new particle.

The most useful channels for the discovery of the Higgs-like boson were $H \rightarrow \gamma\gamma$ [3–6] and $H \rightarrow ZZ^* \rightarrow 4\ell$ [7–10]. Each of these discovery channels has strengths and weaknesses. For example, observation of the appropriate excess in diphoton events immediately implies that the discovered resonance is not spin one [11, 12]. At the same time, because of the much larger background, measuring the exact properties of the object in $\gamma\gamma$ events will be quite challenging [13–19].

In contrast, the “golden channel”¹ $H \rightarrow ZZ^* \rightarrow 4\ell$ offers the opportunity of clean measurements of the mass, spin, parity, etc. of the new resonance in a controlled environment with low backgrounds. Furthermore, the more complex four lepton final state allows experiments to probe the polarization of the intermediate Z bosons through angular correlations. Thus most previous theoretical work on spin and parity discrimination has concentrated on this channel [13, 17, 20–36]; see also [37–41]. In most of this previous work, the availability of a clean signal sample has been assumed. With the exception of Ref. [42], relatively little effort has gone into the important prior question of discriminating between the Higgs signal and the SM background in this channel. This is currently a pressing issue, especially because for a SM Higgs with mass near 125 GeV, the branching fraction into ZZ^* is kinematically suppressed, which leads to comparable signal and background rates. Another motivation for revisiting previous work on this channel is that much of the previous literature is limited to the case of a heavy Higgs mass, above the ZZ threshold, where both Z bosons are on-shell.

As noted above, one of the great advantages of the golden channel is that the final state is fully reconstructed and well-measured, in contrast to channels with missing neutrinos, e.g. $H \rightarrow WW^*$, where the selection of optimal kinematic variables is an ongoing question [43–47]. Additionally, the presence of four leptons in the final states means that, at leading order, there are eight independent observed degrees of freedom (in the Higgs CM frame), not counting the irrelevant azimuthal orientation of the event. The existence of eight meaningful kinematic variables strongly motivates the use of a Multivariate Analysis (MVA) [48], thereby allowing all of the information in each event to be used in distinguishing signal from the background, in particular the irreducible $pp \rightarrow (Z/\gamma^*)(Z/\gamma^*) \rightarrow 4\ell$ background, which we will consider here. Reducible backgrounds could presumably be dealt with using control regions (as in Ref. [10]).

A particularly natural choice of MVA for the golden channel is the Matrix Element Method (MEM) [17, 31, 32, 42, 49, 50]. In this method, the squared matrix element for producing the observed final state in a given process is used either to form a test statistic or to construct the likelihood directly. This method has several advantages over other MVAs. The quantity used in the analysis is the (squared) matrix element, which is (up to technical complications, higher order corrections, etc.) uniquely defined. Unlike boosted decision trees or neural network methods, the MEM is not (in principle) dependent on a set of Monte Carlo events on which the analysis is trained; while these other MVA can presumably achieve an identical level of discrimination, a large amount of simulation would be needed

¹Throughout this paper we shall use the notation where Z stands for both on-shell and off-shell Z -bosons, as well as γ^* , while Z^* stands for either an off-shell Z or γ^* . In other words, we never make an on-shell Z approximation.

in order to have a meaningful training in the 8 parameter phase space. Additionally, since the matrix element has a clear, well-understood physical meaning, one is able to make a direct connection between the features of a statistical analysis and the underlying physics. This is particularly true in the case of the golden channel, as the distributions of kinematic variables can be determined from the amplitudes for producing Z bosons of given helicity [51, 52].

Finally, there are commonly used and well-tested programs which can be utilized to calculate the matrix element automatically [53]. These include tools to generate model files from an arbitrary Lagrangian, such as FeynRules [54] and LanHEP [55], as well as tools to calculate the matrix elements using these model files, such as MadGraph [56, 57], CalcHEP [58], and CompHEP [59, 60]. Taken together, these tools allow for relatively automatic implementation of new models and automatic generation of matrix elements, as explained at the TASI-2011 summer school [61] and the MC4BSM-2012 workshop [53, 62]. The existence of such tools strongly motivates the use of the MEM where possible.

The goal of this paper is to demonstrate the use of these automated tools for performing a MEM analysis of signal versus background discrimination in the physically important and timely example of the Higgs golden channel $H \rightarrow ZZ^* \rightarrow 4\ell$. First in Section 2 we review the MEM and describe the associated variable, the kinematic discriminant KD , which quantifies how signal-like a particular event is. We also show the superiority of the MEM over analyses involving fewer variables. In the next four sections, we calculate KD for signal and background events using three different tools: MADGRAPH [57] in Section 3, CALCHEP [58] in Section 4, and MCFM [63, 64] in Section 5. We emphasize that we are limited to considering publicly available tools, as only such tools may be employed in phenomenological analyses. Section 6 compares the discrimination power of the kinematic discriminants computed with those three tools. In Section 7, we discuss the added benefit from incorporating into the analysis the known information about the initial state. The idea is to take advantage of the fact that, at leading order, the Higgs boson is produced mainly from a gg initial state, while the SM background is initiated by a $q\bar{q}$ pair. This difference between the initial state partons will then be reflected in the rapidity distribution of the event in the LAB frame. Section 8 summarizes our findings and outlines directions for future work. Appendix A introduces the notation for the relevant kinematic variables in the Higgs golden channel and contrasts the shapes of their distributions for signal and background. In order to facilitate future MEM-based studies of the properties of the newly discovered four lepton resonance by the experimental and theoretical communities, we are making public one of the two new KD codes used in this paper (the MADGRAPH-based code used for Section 3), with instructions on how to install and run the code given in Appendix B.

2 Preliminaries

We now define the MEM and note some modifications to the general procedure which are useful in studying the golden channel. We then describe a practical method for displaying the sensitivity of different kinematic discriminants. Finally we use the Higgs golden channel

in a toy example to demonstrate the increase in discrimination power that may be obtained using the MEM, as compared with analyses which use fewer variables.

2.1 The matrix element method and its kinematic discriminant KD

It is natural to assume that an experimental analysis will gain greater sensitivity when more information from the observed events is used in the analysis. When constructing a log-likelihood ratio to compare the hypothesis that there is some signal (“s”) and some background (“b”) present to the hypothesis that only background is present, one finds that the dependence on event-by-event information is through the quantity

$$D(\theta_s; \theta_b; \mathbf{x}_i) = \frac{P_s(\theta_s; \mathbf{x}_i)}{P_b(\theta_b; \mathbf{x}_i)}. \quad (2.1)$$

Here $P_{s(b)}(\theta_{s(b)}; \mathbf{x}_i)$ is the (normalized) probability of observing an event described by kinematic information \mathbf{x}_i in the signal (background) hypothesis; $\theta_{s(b)}$ are parameters of the signal (background) model. In particle physics, it is natural to think of these probabilities as representing the differential cross section of a signal or background process with respect to the variables considered, normalized by the appropriate total cross section. Thus, an explicit expression for $P_{s(b)}(\theta_{s(b)}; \mathbf{x}_i)$ as a function of all final state momenta p_i , and initial state partons q_1 and q_2 is provided by

$$\frac{\sum_j \mathcal{P}_j(p_i) f_{q_1,j}^p(x_1) f_{q_2,j}^p(x_2) \left| \mathcal{M}_{s_j(b_j)}(p_i) \right|^2}{\sum_j \int \prod_i d\mathbf{p}_i \mathcal{P}_j(p_i) \int dx_1 dx_2 f_{q_1,j}^p(x_1) f_{q_2,j}^p(x_2) \left| \mathcal{M}_{s_j(b_j)}(p_i) \right|^2}. \quad (2.2)$$

Here j labels processes with distinct initial states, $\int \prod_i d\mathbf{p}_i \mathcal{P}_j(p_i)$ is the integral over phase space, $f_{q_1,j}^p(x_1)$ and $f_{q_2,j}^p(x_2)$ are the relevant parton distribution functions, and $\left| \mathcal{M}_{s_j(b_j)}(p_i) \right|^2$ is the squared matrix element for the signal (background) process labelled by j . We note that we are only interested in the ratio of $P_s(\theta_s)$ and $P_b(\theta_b)$, and many of the terms in Eq. 2.2 will cancel in the ratio. If all signal and background processes involve effectively massless initial state partons (as is often the case), the phase space factors are identical for all signal and background processes and hence will cancel in the ratio. Thus up to an overall normalization (which includes the ratio of total signal and background cross sections, as well as potential differences in color or symmetry factors) we find that

$$D(\theta_s; \theta_b; \mathbf{x}_i) \propto \frac{\sum_j f_{s_j,q_1}^p(x_1) f_{s_j,q_2}^p(x_2) \left| \mathcal{M}_{s_j}(p_i) \right|^2}{\sum_k f_{b_k,q_1}^p(x_1) f_{b_k,q_2}^p(x_2) \left| \mathcal{M}_{b_k}(p_i) \right|^2}, \quad (2.3)$$

The product of parton distribution functions in the numerator and denominator in general will not cancel; in particular they do not cancel in the case of $ZZ^* \rightarrow 4\ell$, as the initial state for the signal is gg , while the initial state for the background is $q\bar{q}$. While we consider only a single process in the numerator $gg \rightarrow H \rightarrow ZZ^* \rightarrow 4\ell$, for the background, at a proton–proton collider like the LHC, we must sum over the expressions corresponding to both the case where the quark (antiquark) carries momentum fraction x_1 (x_2) and the case where the antiquark (quark) has momentum fraction x_1 (x_2). We must also sum over all relevant

flavors of quarks. Each matrix element (for a given signal or background process) involves the sum over all diagrams for the given process. In particular, both the amplitudes for $q\bar{q} \rightarrow ZZ^* \rightarrow 4\ell$ and for $q\bar{q} \rightarrow Z\gamma^* \rightarrow 4\ell$ must be considered in calculating the background. However, for convenience, we will always refer to all resonances in this paper as “Zs”.

Note that Eq. 2.3 is invariant under any changes of variables in the expressions in Eq. 2.2, as any resulting Jacobian would be common to both the signal and background expressions, and hence would cancel in the ratio.

In general, there are two complications in using the matrix element, which we have ignored thus far.

1. Not all particles in the final state may be observed.
2. The momenta of final state particles are not perfectly measured.

Item 1 is not relevant for the golden channel. However we note that in general, if some particles in the final state are not observable (such as neutrinos or neutralinos), then it is also necessary to integrate over the potential momenta of these particles; this integration can be performed in an optimized way from automatically generated matrix elements in the MADWEIGHT package [57, 65].

However, item 2 is an issue for this channel. Generally one takes this into account by including an integration over transfer functions for the final state momenta in both the numerator and denominator of Eq. 2.2; these integrals do not cancel in the ratio. Since leptons are well-measured, one can use delta function transfer functions for many applications involving leptons in the final state. However, this is not true, strictly speaking, for the case in which the signal process is the production of a narrow resonance, since the value of the signal matrix element will be very sensitive to small perturbations in the measured invariant mass when the measured invariant mass is in the neighborhood of the resonance mass. This is true of the channel we are considering: the width of a 125 GeV SM Higgs boson is only a few MeV [66].

This was taken into account in the CMS $H \rightarrow ZZ^* \rightarrow 4\ell$ analysis for ICHEP [9, 10] by using matrix element information as well as the invariant mass shape to construct a two dimensional likelihood. This allows the broadening of the resonance due to instrumental effects to be taken into account; a procedure such as this must be employed if more realistic transfer functions are not used. In what follows, we will assume that such a procedure has been employed; we will not consider transfer functions further in the rest of this work.

Once the event invariant mass is a separate independent input to the analysis, for the MEM discriminant one can set $M_H = M_{4\ell}$ [9, 10], thus avoiding the problem that the Higgs boson mass M_H is a priori unknown. In what follows, we will therefore consider two quantities useful for the calculation of the discriminant in Eq. 2.3, namely

$$f \circ KD(p_i; M_{4\ell}) \equiv \ln \left(\frac{f_g^p(x_1)f_g^p(x_2)|\mathcal{M}_{SIG}(p_i; M_{4\ell})|^2}{\sum_q [f_q^p(x_1)f_q^p(x_2)|\mathcal{M}_{BKG}(p_i)|^2 + (q \leftrightarrow \bar{q})]} \right) \quad (2.4)$$

and

$$KD(p_i; M_{4\ell}) \equiv \ln \left(\frac{|\mathcal{M}_{SIG}(p_i; M_{4\ell})|^2}{|\mathcal{M}_{BKG}(p_i)|^2} \right). \quad (2.5)$$

For simplicity, from now on we shall omit the arguments of KD and only use an index to specify which software program has been used to evaluate the matrix elements and subsequently the kinematic discriminant KD , e.g., KD_{MAD} means that the functions $\mathcal{M}(p_i)$ have been evaluated with MADGRAPH, etc.

We reiterate that, following the procedure used in the CMS analysis for ICHEP, we do not use as our signal hypothesis a Higgs with a specific mass. Rather, when calculating quantities such as KD for a given event, we set the Higgs mass to the invariant mass $M_{4\ell}$ of that given event. While this may obscure any direct interpretation of KD in terms of the log-likelihood which one could construct directly from the KD , this is not, in itself, an issue as one ultimately constructs a two dimensional likelihood in $(M_{4\ell}, KD)$.

A potential concern with calculating KD using $M_H = M_{4\ell}$ is that the normalization in Eq. 2.3 is now a function of the Higgs mass. In an unbinned analysis, or in the limit where the normalization can be treated as constant within a bin, this variable normalization will have no effect on the significance obtained from a two dimensional likelihood involving KD and invariant mass, provided the normalization has no dependence on any other kinematic variable. Of course for finite bin width, one should quantify the effects of different choices of normalization using pseudo-experiments; we will not discuss this question further.

2.2 ROC curves

We wish to characterize the extent to which our KD will be useful in enhancing the sensitivity of an analysis. Obviously, one could e.g., perform pseudo-experiments using the two-dimensional likelihood (involving KD and invariant mass $M_{4\ell}$) described above. However a simpler and more intuitive means of displaying the extent to which signal and background may be separated is provided by ROC curves.

“Receiver Operating Characteristic” or “ROC” curves can be constructed as follows. One calculates KD for a large set of signal events and a large set of background events. Clearly some event has lower KD than any other event in either event set; we term this value KD_{MIN} . Likewise, some event will have greater KD than any other event; we term this value KD_{MAX} . We now consider the effect of imposing a cut, $KD \geq KD_{\text{CUT}}$, on both the signal and background event sets. Clearly, the fraction of signal events with $KD \geq KD_{\text{MIN}}$ is 1.0 as is the fraction of background events with $KD \geq KD_{\text{MIN}}$. This corresponds to the point (1.0, 1.0) in a plane where one axis is the signal fraction and the other axis is the background fraction of events that survive a given cut $KD > KD_{\text{CUT}}$. We then smoothly increase KD_{CUT} from KD_{MIN} to slightly greater than KD_{MAX} . Clearly, KD_{CUT} parameterizes a curve in this space for which every point gives the fraction of signal events which pass a given cut on KD in terms of the fraction of background events which pass the same given cut on KD , and vice versa.

2.3 Event generation

For the analyses described below, we use parton-level events generated with MADGRAPH [57, 67, 68]. Both signal and background events were generated within the Higgs mass window $120 < M_{4\ell} < 130$ GeV. When generating the signal, we use a nominal Higgs mass of $M_H = 125$ GeV. For background ZZ events, only processes initiated by first two

generation quarks were generated. The lepton acceptance cuts were: $p_T(e) > 7$ GeV and $|\eta(e)| < 2.5$ for electrons, and $p_T(\mu) > 5$ GeV and $|\eta(\mu)| < 2.4$ for muons [10].

Events are generated for each possible choice of final state flavors, namely $e^-e^+\mu^-\mu^+$ (“opposite flavor”), and $e^-e^+e^-e^+$ and $\mu^-\mu^+\mu^-\mu^+$ (“same flavor”). In the case of opposite flavor lepton pairs with invariant masses M_{Z1} and M_{Z2} (which are defined so that $M_{Z1} > M_{Z2}$) we demand that $M_{Z1} > 40$ GeV, while $M_{Z2} > 12$ GeV [10]. In the case where all four final state leptons are of the same flavor, we accept the event if at least one pairing of leptons passes the invariant mass cuts. We do not perform any detector simulation as our primary concern is with the comparison of the different analyses as opposed to the absolute performance of any given analysis.

2.4 Comparison with single variable analyses

The most sensitive kinematic variable for distinguishing signal and background is, of course, the invariant mass of the event. In fact the analysis presented at ICHEP by the ATLAS collaboration [7, 8] relies only on invariant mass information. However, if we want to move beyond this and obtain greater sensitivity, a natural question is whether we truly need to use all of the kinematic variables in our analysis, or whether using one or two particularly sensitive variables would suffice. We therefore investigate several angular variables, in the convention of Refs. [17, 31], as well as M_{Z2} , the mass of the less massive Z boson. We choose M_{Z2} , as due to the $Z\gamma^*$ contribution to the background, the signal and background shapes are significantly different. The angle θ^* is chosen, as the background is much more peaked in forward and backward direction, while the angle Φ , which corresponds to the angle between decay planes, has often been considered in the literature for distinguishing between spin and parity hypotheses (see, e.g., Refs. [20, 24]). The distributions of signal and background events with respect to these quantities are shown in Figure 9 in Appendix A.

For each of these variables, which we label x , we construct histograms of the signal and background events for this variable, which are used to construct numerically $P_s(x)$ and $P_b(x)$. We then take the ratio of these probabilities and construct the ROC curves accordingly. (The ratio is used as KD in the procedure described in 2.2). These ROC curves are shown in Fig. 1, along with the ROC curve constructed using the MEM as calculated by MADGRAPH (see Sec. 3 for details). We note that the MEM is the most sensitive analysis, though M_{Z2} is very sensitive in its own right.

2.5 Overview of available tools for calculating KD

Since an event generator is performing a Monte Carlo integration of a matrix element squared over the relevant phase space, in principle *any* event generator can be used as a matrix element calculator, given the final state kinematics. Unfortunately, not all event generators have implemented this functionality. For the case of the golden channel, we are limited to the tools contrasted in Table 1.

Table 1 focuses on the five features where (some of) the tools differ. MADGRAPH, CALCHEP and MCFM provide the analytic matrix element for the corresponding $2 \rightarrow 4$ scattering process, $gg \rightarrow H \rightarrow ZZ^* \rightarrow 4\ell$ for signal and $q\bar{q} \rightarrow ZZ^* \rightarrow 4\ell$ for the

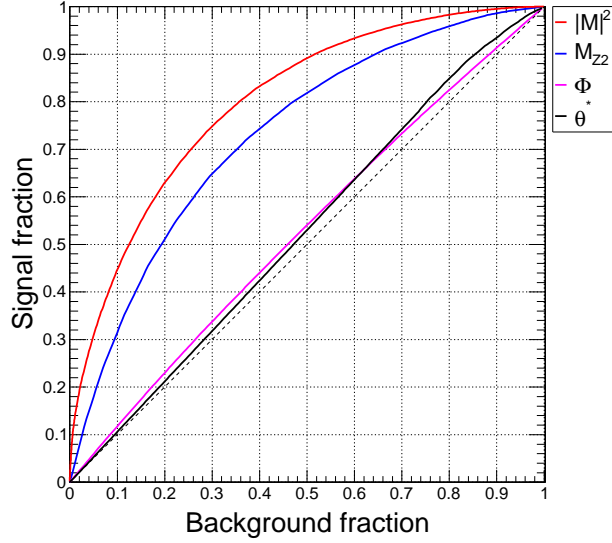


Figure 1. Comparison of the ROC curve obtained using the value of KD obtained from matrix elements (red curve) with the ROC curve obtained from single variable distributions for the variables M_{ZZ} (blue curve), Φ (magenta curve), and θ^* (black curve). The black dashed line gives the ROC curve obtained from cutting events indiscriminately (e.g., by flipping a fair coin or by only considering some fraction of a data set).

Feature	MADGRAPH	CALCHEP	MCFM/NLOME	MELA
ME event topology	$2 \rightarrow 4$	$2 \rightarrow 4$	$2 \rightarrow 4$	$1 \rightarrow 4$
ME for signal	yes	yes	only for OF	NWA
ME for background	yes	yes	only for OF	approximations
Initial state pdf	yes	yes	yes	no
NLO capability	no	no	yes	no

Table 1. Comparison of the functionality of different matrix element KD calculators. “OF” refers to “opposite flavor”, i.e., the $e^-e^+\mu^-\mu^+$ final state. “NWA” refers to the narrow width approximation.

background. On the other hand, the MELA package [10, 17, 31, 69] computes the matrix element for a $1 \rightarrow 4$ decay process for the $H \rightarrow ZZ^* \rightarrow 4\ell$ signal, while for the background, in the mass range of interest, instead of analytical parametrisation, the background is tabulated in a correlated template distribution using POWHEG simulation at generator level [10, 69] (although efforts are underway to extend the existing analytical matrix element for the background below the ZZ threshold [69]).

At the same time, unlike MADGRAPH or CALCHEP, MCFM is not an automated matrix element calculator, and can only rely on the already existing expressions coded in it. In the case of the Higgs golden channel, MCFM currently contains only the matrix element for the opposite flavor (OF) $e^-e^+\mu^-\mu^+$ final state. With suitable replacements, one could use the OF matrix element and try to build an approximation for the same flavor

(SF) case, but that would miss the interference terms. Nevertheless, as we shall show below in Section 5, such an approach works out numerically rather well.

In the Introduction, we alluded to the possibility of using the available information about the initial state (through the measured parton momentum fractions x_1 and x_2) to improve the discrimination between signal and background. To this end, one must weigh the usual matrix element by the parton distribution functions as in Eq. 2.4. This functionality, however, is only available in MADGRAPH, CALCHEP and MCFM. Finally, the one advantage of MCFM over all other tools is that MCFM is already an NLO tool. In principle, MADGRAPH, CALCHEP and MELA could also be adapted to NLO for the Higgs golden channel, but this would require some effort.

As Table 1 demonstrates, there is no single tool which is “best” — different tools have different advantages and disadvantages. Nevertheless, to the extent that we are concerned with the leading order case (as in this paper), it appears that MADGRAPH and CALCHEP are the two tools of choice, so we shall start with them in the next two sections.

3 KD from MADGRAPH

We used MADGRAPH to obtain a code to calculate the kinematic discriminants KD and $f \circ KD$. The code is publicly available [70] and instructions for download and usage are provided in Appendix B. The code is based on the SM, implemented into MADGRAPH via FEYNRULES [54]. In addition, we also allow for non-SM Higgs couplings. Following [17, 31], we implement the following additional terms in the Lagrangian:

$$\mathcal{L}_{HZZ} \ni -\frac{g_{1z}}{2} H Z_\mu Z^\mu - \frac{g_{2z}}{4} H Z_{\mu\nu} Z^{\mu\nu} - \frac{g_{3z}}{2} Z_{\mu\alpha} Z^{\mu\beta} (\partial_\beta \partial^\alpha H) - \frac{g_{4z}}{4} H Z_{\mu\nu} \tilde{Z}^{\mu\nu}, \quad (3.1)$$

$$\mathcal{L}_{HGG} \ni -\frac{g_{1g}}{2} H G_\mu^a G^{a,\mu} - \frac{g_{2g}}{4} H G_{\mu\nu}^a G^{a,\mu\nu} - \frac{g_{3g}}{2} G_{\mu\alpha}^a G^{a,\mu\beta} (\partial_\beta \partial^\alpha H) - \frac{g_{4g}}{4} H G_{\mu\nu}^a \tilde{G}^{a,\mu\nu} \quad (3.2)$$

so that the complete Lagrangian reads

$$\mathcal{L} \equiv \mathcal{L}_{SM} + \mathcal{L}_{HZZ} + \mathcal{L}_{HGG}. \quad (3.3)$$

Note that the SM Higgs couplings are already included in the SM Lagrangian \mathcal{L}_{SM} , so that the couplings g_i are the *deviations* from the SM expectations, so that the SM limit is obtained as $g_i \rightarrow 0$. The user has complete freedom to adjust the scalar (g_1, g_2 and g_3) and pseudoscalar (g_4) couplings, so that the code can also be used for parity studies.

4 KD from CALCHEP

Similarly, we also created an independent code to compute KD_{CALC} , where the matrix element is calculated by CALCHEP. As in the previous section, the SM was implemented via FEYNRULES, which ensures that our KD_{MAD} and KD_{CALC} results are obtained with identical inputs for the SM parameters (masses, couplings, etc.). As we already saw from Table 1, there are no functionality differences between MADGRAPH and CALCHEP, so one would expect that KD_{MAD} and KD_{CALC} should be the same.

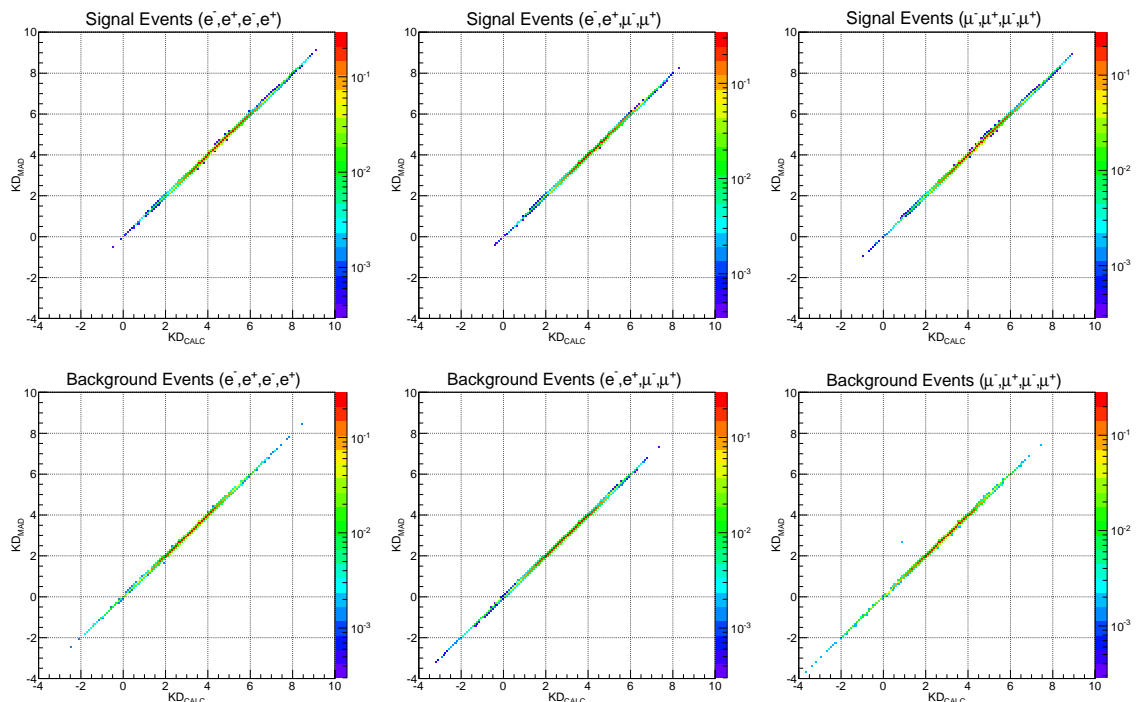


Figure 2. Comparison of the kinematic discriminant, KD_{CALC} , computed with CALCHEP and the kinematic discriminant, KD_{MAD} , computed by MADGRAPH for signal events (top row) and background events (bottom row), using $4e$ events (left column), 4μ events (right column), and $2e2\mu$ events (middle column).

Indeed, this exercise provides a useful sanity check for our implementations. We performed consistency checks on both of our signal and background samples, for opposite flavor as well as same flavor final states. The results are displayed in Fig. 2, which reveals that, as expected, KD_{MAD} and KD_{CALC} are in excellent agreement (as are the signal and background matrix elements as calculated by the two tools). This synchronization exercise serves a dual purpose: first, we are able to validate our code, and second, the level of agreement seen in Fig. 2 provides a benchmark for the comparisons to follow in the next two sections.

5 KD from MCFM

The MCFM code [63] can be inverted to compute the matrix element weight $|\mathcal{M}|^2$ from a given final state kinematic configuration. The corresponding code, NLOME [64], is still under development. Here we use a beta version of NLOME² to cross-check against our results from the previous two sections. We should mention that as a NLO tool, NLOME involves an integration over the unknown longitudinal momentum of the additional jets, which are recoiling against the 4ℓ system. However, here we are using LO events, since we

²We thank J. Campbell and C. Williams for making the beta version of the NLOME code available to us.

are interested in comparing the *leading order* machinery implemented in the different tools. This is why we removed the additional longitudinal momentum integration in NLOME and we are running the MCFM/NLOME code in a purely LO mode.

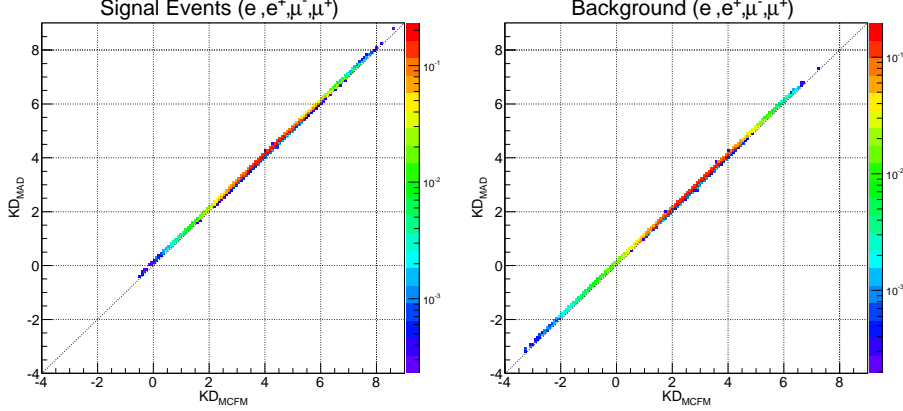


Figure 3. Comparison of the kinematic discriminants KD_{MCFM} and KD_{MAD} for different flavor $2e2\mu$ events for signal (left plot) and background (right plot).

The comparison between KD_{MAD} and KD_{MCFM} for opposite flavor 4ℓ events is shown in Figs. 3. (We do not show a comparison between KD_{CALC} and KD_{MCFM} because we already saw in Fig. 2 that the KD_{CALC} and KD_{MAD} results are essentially identical.) We begin with opposite flavor events because, according to Table 1, that is the case when the two calculations are on equal footing and their results should agree. Indeed, this is what Fig. 3 shows: the level of agreement is excellent and comparable to what we observed earlier in Fig. 2.

However, as we already discussed in Sec. 2.5, currently MCFM does not have the full matrix element for same flavor 4ℓ events, and one must patch the existing code somehow. Our procedure for same flavor events is to recycle the opposite flavor matrix element

$$|\mathcal{M}_{OF}(e^- e^+ \mu^- \mu^+)|^2$$

and write

$$|\mathcal{M}_{SF}(e_1^- e_1^+ e_2^- e_2^+)|^2 \approx |\mathcal{M}_{OF}(e_1^- e_1^+ e_2^- e_2^+)|^2 + |\mathcal{M}_{OF}(e_2^- e_1^+ e_1^- e_2^+)|^2, \quad (5.1)$$

which, of course, misses the interference terms.

In order to see the size of the effect of neglecting the interference, in Fig. 4 we compare three quantities; the signal matrix element (left column), the background matrix element (middle column), and the kinematic discriminant (right column), calculated in two different ways with MADGRAPH. The x axis shows the full result for SF events from MADGRAPH, while the y axis shows the result from the patch Eq. 5.1. Fig. 4 shows a good overall agreement, which gets worse for low values of the squared matrix element. This can be easily understood — for SF events, there are two amplitudes corresponding to the two ways of pairing the final state leptons. Normally one pairing has one Z on-shell and the other

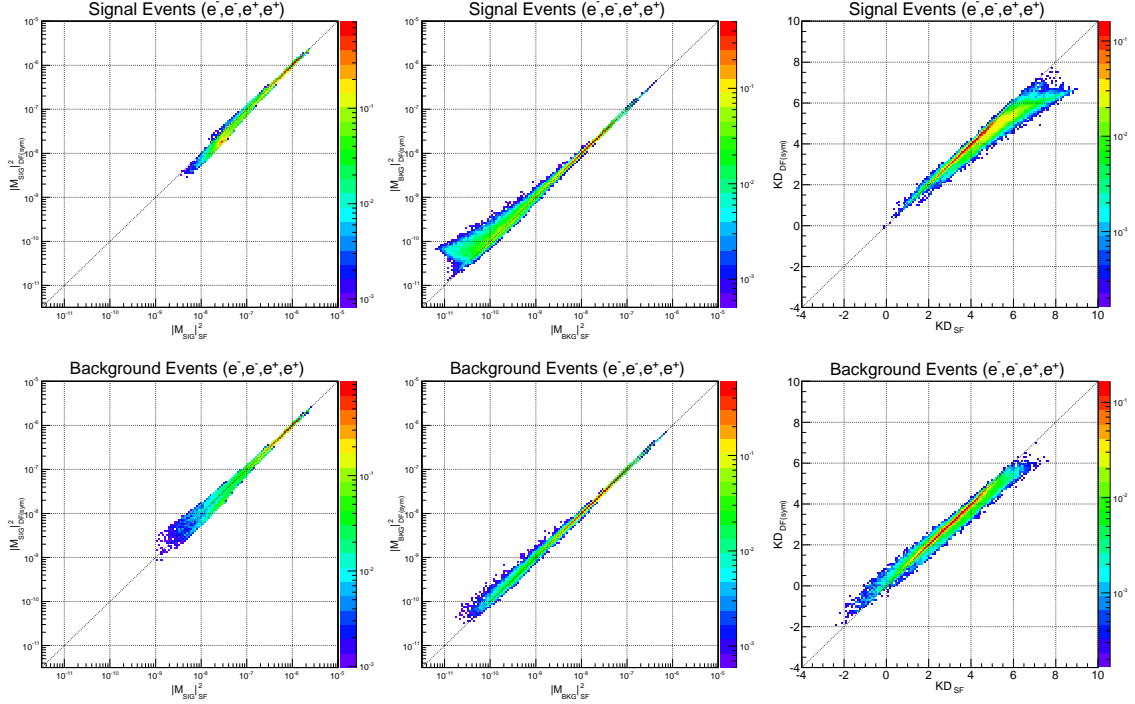


Figure 4. Comparison of the signal (left column) and background (middle column) matrix element, as well as the kinematic discriminant KD_{MAD} (right column), for signal events (top row) and background events (bottom row) as calculated with the full matrix element for SF events $|\mathcal{M}|_{\text{SF}}^2$ (including the interference) versus the approximation $|\mathcal{M}|_{\text{DF(sym)}}^2$ obtained by the patch (5.1). All quantities are calculated with MADGRAPH.

Z off-shell, while the other pairing has both Z 's off-shell. Then the result is dominated by the on-shell amplitude squared and the interference terms are negligible. In order for them to become noticeable, both pairings should have *two* off-shell Z 's in which case the overall matrix element squared will be small. We can easily observe this effect, especially for the background matrix element (the middle plots in the figure), which has a γ^* interference and more easily allows the Z 's to be off-shell. The larger spread at low $|\mathcal{M}_{\text{BKG}}|^2$ appears at high KD (right column plots), since the KD ratio is inversely proportional to $|\mathcal{M}_{\text{BKG}}|^2$.

6 Performance summary

Having obtained three different implementations of the LO kinematic discriminant KD in the previous three sections, we are now in position to compare the sensitivities of the respective MEM analyses using each version of KD . As discussed in Sec. 2.2, the effectiveness of the method can be measured by the ROC curves in Fig. 5. The figure shows that the ROC curves for KD_{MAD} , KD_{CALC} and KD_{MCFM} for opposite flavor events are essentially identical, as expected from the earlier comparisons in Sections 4 and 5. For SF events, there is a very slight difference between KD_{MAD} and KD_{CALC} , on the one hand, and KD_{MCFM} , which is due to the approximation (5.1), as discussed in Fig. 4. The

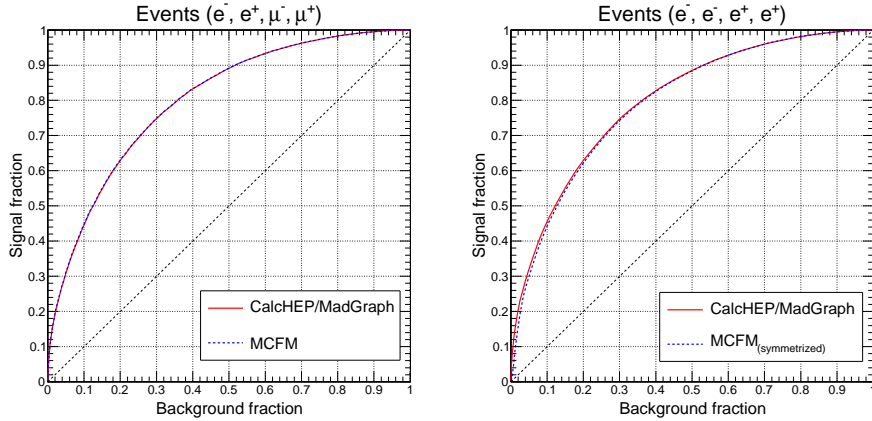


Figure 5. Comparison of ROC curves obtained from the different implementations of the kinematic discriminant: KD_{MAD} from MADGRAPH, KD_{CALC} from CALCHEP, and KD_{MCFM} from MCFM, for OF 4ℓ events (left) and SF events (right).

agreement observed in Fig. 5 is very encouraging and validates our implementations.

7 Improvement by including information about the initial state

In the Higgs golden channel, the final state is fully reconstructed and thus we also know the momenta of the initial state partons. In all of our discussion so far, we have been ignoring this additional information, so a very relevant question is how much does one gain from considering $f \circ KD$ in place of KD . To illustrate the idea, in Fig. 6 we plot the rapidity distributions for signal and background events generated with PYTHIA [71] at the two relevant LHC energies. The dashed histograms represent parton-level distributions before cuts. We notice a substantial difference in the shapes of the signal and the background — the Z -bosons in the background events are much more forward, which is due to the fact that they are produced from an asymmetric $q\bar{q}$ state, where typically the quark carries a larger momentum fraction, x . In contrast, the signal distributions are much more central, since the Higgs boson is produced from a symmetric gg initial state, where the gluons are likely to share the momentum more evenly.

Unfortunately, these conclusions are modified in the presence of cuts (solid histograms in Fig. 6). The leptons produced in the decays of Z 's at high rapidity are much more likely to fail the lepton acceptance cuts, which shaves off the high rapidity tail in the background distributions. As a result, the signal and background rapidity distributions become similar, but not identical. It is therefore worth asking how much we gain by utilizing the residual rapidity differences observed in the figure.

To this end, in Fig. 7 we compare the ROC curves obtained from KD (red lines) and $f \circ KD$ (blue lines). In the absence of cuts (dashed lines), the difference between the two ROC curves is quite significant, as one might have guessed from Fig. 6. However, after cuts (solid lines), the curves become quite similar and the advantage of using $f \circ KD$ can be quantified as being at the percent level.

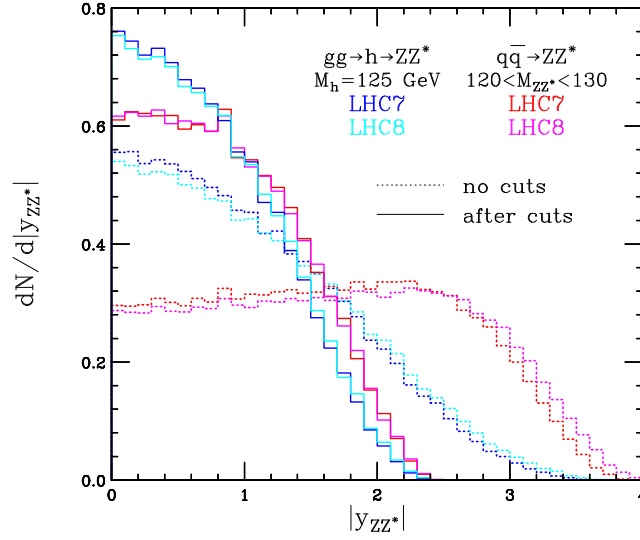


Figure 6. Unit-normalized rapidity distributions of ZZ^* events for signal (bluish colors) and background (reddish colors). Results are shown for two different LHC energies (7 and 8 TeV), before cuts (dashed lines) and after cuts (solid lines).

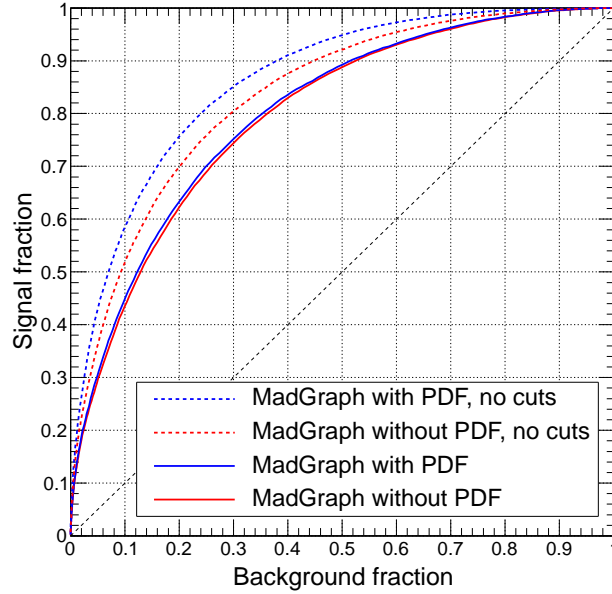


Figure 7. Impact of parton distribution functions on ROC curves. The red curves are based on KD_{MAD} and do not account for the longitudinal boost of the event, while the blue curves are based on $f \circ KD_{\text{MAD}}$ and include the effect from the parton distribution functions. Solid (dashed) lines are obtained from event samples with (without) cuts.

8 Summary and outlook

We believe that the Higgs golden channel $H \rightarrow ZZ^* \rightarrow 4\ell$ is ideally suited for the application of the matrix element method. We have shown that a MEM-based analysis improves the extent to which signal can be discriminated from the background. A major component of the work presented here is the development and validation of computer tools for calculating the MEM kinematic discriminant using standard high energy physics software. One of these tools (the KD_{MAD} calculator) is now publicly available [70]; the other tools are also available upon request. We note that those codes are capable of studying not just the SM Higgs boson, but a general spin zero resonance, and in the near future will be utilized for spin and parity measurements as well.

We restricted the discussion in this paper to leading order for greater clarity and to better focus the discussion on the comparison of the different physics tools. A natural extension of the work presented here is to NLO along the lines of [49, 50, 72]. NLO versions of our MADGRAPH and CALCHEP codes for KD will be presented in a forthcoming work [73]. The availability of alternative simulation and analysis tools in high energy physics has always been a virtue which stimulates progress.

Acknowledgments

We thank A. Gritsan for useful correspondence. J. Gainer and K. Matchev thank the Aspen Center for Physics (funded by NSF Grant #1066293) for hospitality during the completion of this work. M. Park is supported by the CERN-Korea fellowship through National Research Foundation of Korea. Work supported in part by a U.S. Department of Energy grant DE-FG02-97ER41029 and NSF grant 1007115.

A Notation and conventions

At leading order, events in the Higgs golden channel are described by 10 degrees of freedom³. Following [17, 31], we can take them to be as follows:

- Three invariant mass parameters: $M_{4\ell}$, M_{Z1} and M_{Z2} .
- The rapidity y_{ZZ^*} of the event in the LAB frame, see Section 7.
- Two angular variables defined in the CM frame of the whole event. Those can be chosen to be the polar angle θ^* (measured from the beam axis) and the azimuthal angle Φ^* of the Z_1 system, as shown in Fig. 8.
- Two angular variables defined in the CM frame of the Z_1 system. Those can be taken to be the azimuthal angle Φ_1 and the polar angle θ_1 (measured from the Z_1 direction in the Higgs CM frame) of the lepton ℓ_1^- produced in the Z_1 decay (refer to Fig. 8).

³There are 4 particles in the final state, whose momenta give $4 \times 3 = 12$ parameters, two of which are removed by transverse momentum conservation.

- Two angular variables defined in the CM frame of the Z_2 system. Those can be taken to be the azimuthal angle Φ_2 and the polar angle θ_2 (measured from the Z_2 direction in the Higgs CM frame) of the lepton ℓ_2^- produced in the Z_2 decay. It is often convenient to trade the angle Φ_2 for $\Phi \equiv \Phi_2 - \Phi_1$.

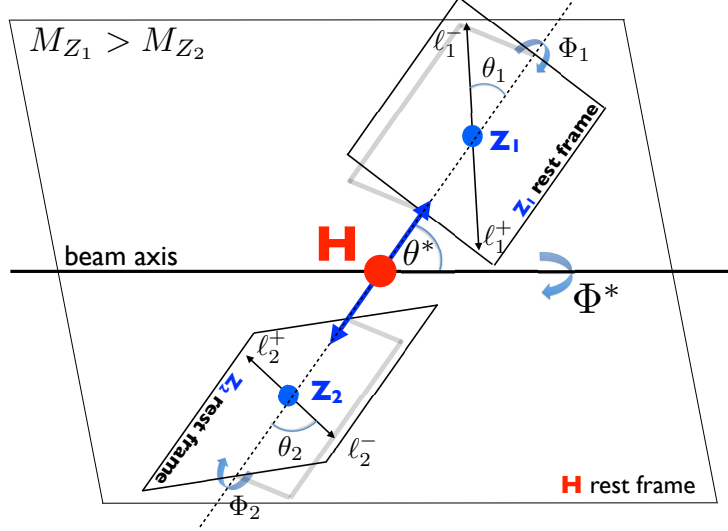


Figure 8. Definition of the angular variables relevant to the $H \rightarrow ZZ^* \rightarrow 4\ell$ event topology.

Having defined the notation for the event kinematics, it is instructive to compare the shapes of the signal and background distributions for these variables. Since the variable y_{ZZ^*} was already considered in Section 7, in Fig. 9 we show unit-normalized distributions for the eight variables M_{Z1} , M_{Z2} , $\cos\theta^*$, Φ^* , $\cos\theta_1$, Φ_1 , $\cos\theta_2$ and Φ . The figure shows that, apart from the conventional choice $M_{4\ell}$, there are a few other variables which can also provide decent signal to background discrimination, above all M_{Z2} and $\cos\theta^*$.

B The Matrix Element (ME) Kinematic Discriminant (KD) Producer

The computer code for calculating KD_{MAD} can be freely downloaded from [70]. The website also includes instructions and examples for installing and running the code, which for completeness are also included here.

B.1 Description of the code

The Matrix Element (ME) Kinematic Discriminant (KD) package provides tools to calculate the leading order (LO) matrix elements for signal $gg \rightarrow X \rightarrow ZZ^* \rightarrow 4\ell$ and background $q\bar{q} \rightarrow ZZ^* \rightarrow 4\ell$ processes, and to build kinematic discriminants KD that can be used for separation between these processes. The supported signal processes include the production of a scalar resonance X through gluon-gluon fusion and its decay into four leptons via two Z gauge bosons, where the couplings of the scalar resonance to gauge bosons are kept general (parametrized). The ME KD package consists of two parts:

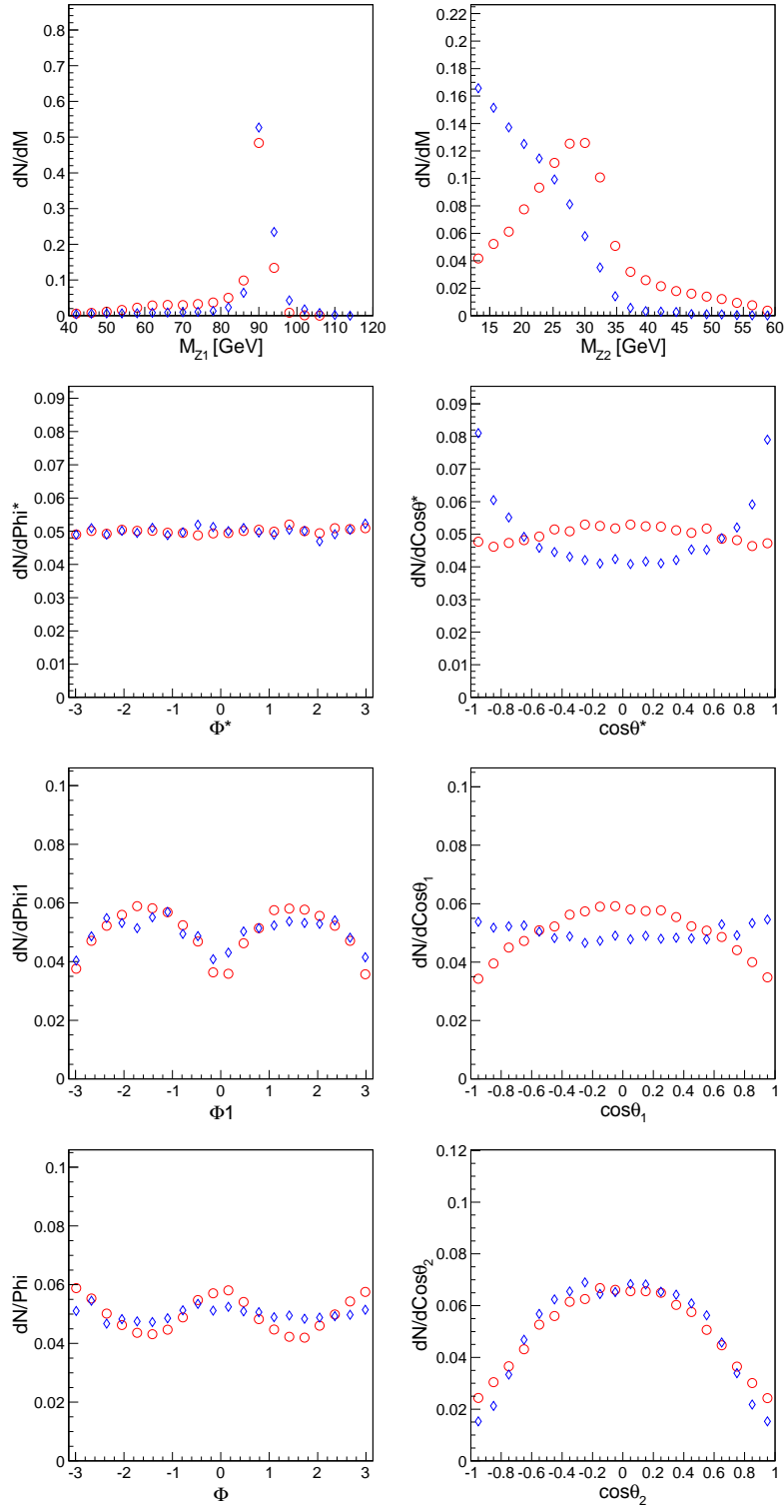


Figure 9. Unit-normalized distributions of signal events (red circles) and background events (blue diamonds) for the 8 kinematic variables discussed in the text.

1. library `meMadgraph.h` (and the corresponding MADGRAPH libraries it depends on);
2. macro/executable code `runKD_MAD.cc`

The library `meMadgraph.h` provides methods to calculate the ME for signal and background processes using the kinematic information about the 4 leptons in the final state. The macro code `runKD_MAD.cc` is an executable that can run over the input sample of 4 lepton events and as an output produces a file with MEs and KDs for each of the input events. Its functionality is based on the library `meMadgraph.h`. The ME KD package provides the following functionalities:

1. Accepts as input the tabulated data file with the kinematic information of 4 leptons in the final state. The format of the input file is the following:

$$id_1 \ id_2 \ id_3 \ id_4 \ p_{1x} \ p_{1y} \ p_{1z} \ e_1 \ p_{2x} \ p_{2y} \ p_{2z} \ e_2 \ p_{3x} \ p_{3y} \ p_{3z} \ e_3 \ p_{4x} \ p_{4y} \ p_{4z} \ e_4$$

where id_N , p_{Nx} , p_{Ny} , p_{Nz} and e_N are the PDG id, spatial components and time component of the Nth lepton 4-momentum, respectively.

2. Allows user to select the PDFs that should be taken into account in ME calculation.
3. Initializes the couplings of the spin 0 resonance according to the user's signal selection.
4. Performs a purely transverse boost of each event to a reference frame where the transverse component of total momenta of the 4-lepton system is zero.
5. Feeds the boosted momenta of all 4 leptons to the ME calculator and computes MEs and the KD for the given event.
6. Provides the output as the tabulated data file with the computed ME and KD values. The format of the output file is the following:

$$|\mathcal{M}_{ZZ}|^2 \ |\mathcal{M}_{XZZ}|^2 \ KD$$

where $|\mathcal{M}_{ZZ}|^2$, $|\mathcal{M}_{XZZ}|^2$ and KD are the squared ME for the background process, the squared ME for the selected signal process and the kinematic discriminant KD , respectively.

7. Prints out the status of the code execution and the summary message at completion.

B.2 User instructions

B.2.1 Requirements

The latest version of the code can be downloaded and installed following the instructions at the ME KD web site:

<http://mekd.ihepa.ufl.edu/>

Compilation of the code requires installed gcc compiler. GCC binary multiple platform packages can be found here:

<http://gcc.gnu.org>

B.2.2 Setup of the ME KD code

In a terminal window, type

```
./setup.sh
```

The script will compile and link all necessary ME KD libraries/macros. One of the outputs is the main executable `runKD_MAD`

B.2.3 Run the ME KD producer

In a terminal window, type

```
./runKD_MAD [-f input_file] [-x x_resonance] [-p pdf_include] [-l log_file]
```

where the available options are described in Table 2. For example, to run the `.dat` file

<code>input_file</code>	name of the input <code>.dat</code> file (string, REQUIRED)
<code>x_resonance</code>	choice of the signal spin-0 resonance (string, DEFAULT = 'Higgs') Available options: Higgs, CP-even and CP-odd.
<code>pdf_include</code>	name of PDFs, PDFs not used if <code>pdf_include=''</code> (string, DEFAULT='')
<code>log_file</code>	name of log file, no logging if <code>log_file=''</code> (string, DEFAULT='')

Table 2. Options of the ME KD producer.

provided in the package, type:

```
./runKD_MAD -f DATA/Events/SIG_4l_30evt.dat
```

and press return. Options and details on input parameters can always be printed out as:

```
./runKD_MAD -h
```

B.2.4 Output from the ME KD producer

To run the code with a user provided input file `yourInputFileName.dat`, do

```
./runKD_MAD -f yourInputFileName.dat
```

and the output will be located in the `.dat` file named

`yourInputFileName_withDiscriminator.dat`

It includes the MEs for selected signal and background, as well as the KD value.

B.2.5 Comparison of user ME KD results

The results of custom user code which uses the `meMadgraph.h` libraries can be compared to the results obtained by the `runKD_MAD.cc` macro. User code should be run on the input `.dat` files (SIG and BKG) which contain 30 events located here:

`DATA/Events`

and the output files with ME KD results can be compared to the reference output files of the "runKD_MAD" macro located in the same directory.

References

- [1] G. Aad *et al.* [ATLAS Collaboration], “Observation of a new particle in the search for the Standard Model Higgs boson with the ATLAS detector at the LHC,” *Phys. Lett. B* **716**, 1 (2012) [arXiv:1207.7214 [hep-ex]].
- [2] S. Chatrchyan *et al.* [CMS Collaboration], “Observation of a new boson at a mass of 125 GeV with the CMS experiment at the LHC,” *Phys. Lett. B* **716**, 30 (2012) [arXiv:1207.7235 [hep-ex]].
- [3] K. Tackmann, “Search for the Higgs boson in the diphoton decay channel with the ATLAS detector”, talk given at the ICHEP 2012 conference, Melbourne, Australia, July 7 2012, <http://indico.cern.ch/contributionDisplay.py?contribId=159&confId=181298>.
- [4] ATLAS Collaboration, “Observation of an excess of events in the search for the Standard Model Higgs boson in the gamma-gamma channel with the ATLAS detector”, ATLAS-CONF-2012-091, <http://cdsweb.cern.ch/record/1460410>.
- [5] S. Ganjour, “Search for SM Higgs decaying to two photons at CMS”, talk given at the ICHEP 2012 conference, Melbourne, Australia, July 7 2012, <http://indico.cern.ch/contributionDisplay.py?contribId=431&confId=181298>.
- [6] CMS Collaboration, “Evidence for a new state decaying into two photons in the search for the standard model Higgs boson in pp collisions”, CMS-PAS-HIG-12-015, <http://cdsweb.cern.ch/record/1460419?ln=en>.
- [7] K. Nikolopoulos “Search for the Standard Model Higgs boson in the $H \rightarrow ZZ^* \rightarrow 4l$ decay channel with the ATLAS detector”, talk given at the ICHEP 2012 conference, Melbourne, Australia, July 7 2012, <http://indico.cern.ch/contributionDisplay.py?contribId=160&confId=181298>.
- [8] ATLAS Collaboration, “Observation of an excess of events in the search for the Standard Model Higgs boson in the $H \rightarrow ZZ^* \rightarrow 4\ell$ channel with the ATLAS detector”, ATLAS-CONF-2012-092, <http://cdsweb.cern.ch/record/1460411>.
- [9] M. Klute, “Search for SM Higgs decaying to ZZ to four leptons at CMS”, talk given at the ICHEP 2012 conference, Melbourne, Australia, July 7 2012, <http://indico.cern.ch/contributionDisplay.py?contribId=433&confId=181298>.
- [10] CMS Collaboration, “Evidence for a new state in the search for the standard model Higgs boson in the H to ZZ to 4 leptons channel in pp collisions at $\sqrt{s} = 7$ and 8 TeV”, CMS-PAS-HIG-12-016, <http://cdsweb.cern.ch/record/1460664?ln=en>.
- [11] L. D. Landau, “On the angular momentum of a two-photon system,” *Dokl. Akad. Nauk Ser. Fiz.* **60**, 207 (1948).
- [12] C.-N. Yang, “Selection Rules for the Dematerialization of a Particle Into Two Photons,” *Phys. Rev.* **77**, 242 (1950).
- [13] W. N. Cottingham and I. B. Whittingham, “Signals of Higgs sector CP violation in neutral Higgs boson decays,” *Phys. Rev. D* **52**, 539 (1995).
- [14] M. C. Kumar, P. Mathews, A. A. Pankov, N. Paver, V. Ravindran and A. V. Tsytinov, “Spin-analysis of s-channel diphoton resonances at the LHC,” *Phys. Rev. D* **84**, 115008 (2011) [arXiv:1108.3764 [hep-ph]].

- [15] A. Alves, E. Ramirez Barreto, A. G. Dias, C. A. de S.Pires, F. S. Queiroz and P. S. Rodrigues da Silva, “Probing 3-3-1 Models in Diphoton Higgs Boson Decay,” *Phys. Rev. D* **84**, 115004 (2011) [arXiv:1109.0238 [hep-ph]].
- [16] J. Ellis and D. S. Hwang, “Does the ‘Higgs’ have Spin Zero?,” arXiv:1202.6660 [hep-ph].
- [17] S. Bolognesi, Y. Gao, A. V. Gritsan, K. Melnikov, M. Schulze, N. V. Tran and A. Whitbeck, “On the spin and parity of a single-produced resonance at the LHC,” arXiv:1208.4018 [hep-ph].
- [18] A. Alves, “Is the New Resonance Spin 0 or 2? Taking a Step Forward in the Higgs Boson Discovery,” arXiv:1209.1037 [hep-ph].
- [19] S. Y. Choi, M. M. Muhlleitner and P. M. Zerwas, “Theoretical Basis of Higgs-Spin Analysis in $H \rightarrow \gamma\gamma$ and $Z\gamma$ Decays,” arXiv:1209.5268 [hep-ph].
- [20] C. A. Nelson, “Correlation Between Decay Planes In Higgs Boson Decays Into W Pair (into Z Pair),” *Phys. Rev. D* **37**, 1220 (1988).
- [21] A. Soni and R. M. Xu, “Probing CP violation via Higgs decays to four leptons,” *Phys. Rev. D* **48**, 5259 (1993) [hep-ph/9301225].
- [22] D. Chang, W. -Y. Keung and I. Phillips, “CP odd correlation in the decay of neutral Higgs boson into ZZ , W^+W^- , or $t\bar{t}$,” *Phys. Rev. D* **48**, 3225 (1993) [hep-ph/9303226].
- [23] T. Arens and L. M. Sehgal, “Energy spectra and energy correlations in the decay $H \rightarrow ZZ \rightarrow \mu^+\mu^-\mu^+\mu^-$,” *Z. Phys. C* **66**, 89 (1995) [hep-ph/9409396].
- [24] S. Y. Choi, D. J. Miller, 2, M. M. Muhlleitner and P. M. Zerwas, “Identifying the Higgs spin and parity in decays to Z pairs,” *Phys. Lett. B* **553**, 61 (2003) [hep-ph/0210077].
- [25] C. P. Buszello, I. Fleck, P. Marquard and J. J. van der Bij, “Prospective analysis of spin- and CP-sensitive variables in $H \rightarrow ZZ \rightarrow l_1^+l_1^-l_2^+l_2^-$ at the LHC,” *Eur. Phys. J. C* **32**, 209 (2004) [hep-ph/0212396].
- [26] S. Schalla, “Study on the Measurement of the CP-Eigenstate of Higgs Bosons with the CMS experiment at the LHC,” IEKP-KA-2004-14.
- [27] R. M. Godbole, D. J. Miller, 2 and M. M. Muhlleitner, “Aspects of CP violation in the HZZ coupling at the LHC,” *JHEP* **0712**, 031 (2007) [arXiv:0708.0458 [hep-ph]].
- [28] V. A. Kovalchuk, “Model-independent analysis of CP violation effects in decays of the Higgs boson into a pair of the W and Z bosons,” *J. Exp. Theor. Phys.* **107**, 774 (2008).
- [29] V. A. Kovalchuk, “Angular correlations and CP asymmetries in the decay $\Phi \rightarrow ZZ \rightarrow 4$ fermions,” *Prob. Atomic Sci. Technol.* **2009N3**, 3 (2009).
- [30] Q.-H. Cao, C. B. Jackson, W.-Y. Keung, I. Low and J. Shu, “The Higgs Mechanism and Loop-induced Decays of a Scalar into Two Z Bosons,” *Phys. Rev. D* **81**, 015010 (2010) [arXiv:0911.3398 [hep-ph]].
- [31] Y. Gao, A. V. Gritsan, Z. Guo, K. Melnikov, M. Schulze and N. V. Tran, “Spin determination of single-produced resonances at hadron colliders,” *Phys. Rev. D* **81**, 075022 (2010) [arXiv:1001.3396 [hep-ph]].
- [32] A. De Rujula, J. Lykken, M. Pierini, C. Rogan and M. Spiropulu, “Higgs look-alikes at the LHC,” *Phys. Rev. D* **82**, 013003 (2010) [arXiv:1001.5300 [hep-ph]].

- [33] C. Englert, C. Hackstein and M. Spannowsky, “Measuring spin and CP from semi-hadronic ZZ decays using jet substructure,” *Phys. Rev. D* **82**, 114024 (2010) [arXiv:1010.0676 [hep-ph]].
- [34] U. De Sanctis, M. Fabbrichesi and A. Tonero, “Telling the spin of the ‘Higgs boson’ at the LHC,” *Phys. Rev. D* **84**, 015013 (2011) [arXiv:1103.1973 [hep-ph]].
- [35] R. Boughezal, T. J. LeCompte and F. Petriello, “Single-variable asymmetries for measuring the ‘Higgs’ boson spin and CP properties,” arXiv:1208.4311 [hep-ph].
- [36] D. Stolarski and R. Vega-Morales, “Directly Measuring the Tensor Structure of the Scalar Coupling to Gauge Bosons,” arXiv:1208.4840 [hep-ph].
- [37] C. Englert, M. Spannowsky and M. Takeuchi, “Measuring Higgs CP and couplings with hadronic event shapes,” *JHEP* **1206**, 108 (2012) [arXiv:1203.5788 [hep-ph]].
- [38] J. Moffat, “Identification of the 125 GeV Resonance as a Pseudoscalar Quarkonium Meson,” arXiv:1207.6015 [hep-ph].
- [39] B. Coleppa, K. Kumar and H. E. Logan, “Can the 126 GeV boson be a pseudoscalar?,” arXiv:1208.2692 [hep-ph].
- [40] P. Cea, “Comment on the evidence of the Higgs boson at LHC,” arXiv:1209.3106 [hep-ph].
- [41] J. Kumar, A. Rajaraman and D. Yaylali, “Spin Determination for Fermiophobic Bosons,” arXiv:1209.5432 [hep-ph].
- [42] J. S. Gainer, K. Kumar, I. Low and R. Vega-Morales, “Improving the sensitivity of Higgs boson searches in the golden channel,” *JHEP* **1111**, 027 (2011) [arXiv:1108.2274 [hep-ph]].
- [43] M. Dittmar and H. K. Dreiner, “How to find a Higgs boson with a mass between 155-GeV - 180-GeV at the LHC,” *Phys. Rev. D* **55**, 167 (1997) [hep-ph/9608317].
- [44] T. Han and R. -J. Zhang, “Extending the Higgs boson reach at upgraded Tevatron,” *Phys. Rev. Lett.* **82**, 25 (1999) [hep-ph/9807424].
- [45] A. J. Barr, S. T. French, J. A. Frost and C. G. Lester, “Speedy Higgs boson discovery in decays to tau lepton pairs : $h \rightarrow \tau\tau$,” *JHEP* **1110**, 080 (2011) [arXiv:1106.2322 [hep-ph]].
- [46] A. J. Barr, B. Gripaios and C. G. Lester, “Re-weighing the evidence for a Higgs boson in dileptonic W-boson decays,” *Phys. Rev. Lett.* **108**, 041803 (2012) [Erratum-ibid. **108**, 109902 (2012)] [arXiv:1108.3468 [hep-ph]].
- [47] A. J. Barr, B. Gripaios and C. G. Lester, “Finding Higgs bosons heavier than $2m_W$ in dileptonic W-boson decays,” *Phys. Lett. B* **713**, 495 (2012) [arXiv:1110.2452 [hep-ph]].
- [48] P. C. Bhat, “Multivariate Analysis Methods in Particle Physics,” *Ann. Rev. Nucl. Part. Sci.* **61**, 281 (2011).
- [49] J. M. Campbell, W. T. Giele and C. Williams, “The Matrix Element Method at Next-to-Leading Order,” arXiv:1204.4424 [hep-ph].
- [50] J. M. Campbell, W. T. Giele and C. Williams, “Extending the Matrix Element Method to Next-to-Leading Order,” arXiv:1205.3434 [hep-ph].
- [51] K. Hagiwara, R. D. Peccei, D. Zeppenfeld and K. Hikasa, “Probing the Weak Boson Sector in $e^+e^- \rightarrow W^+W^-$,” *Nucl. Phys. B* **282**, 253 (1987).
- [52] M. J. Duncan, G. L. Kane and W. W. Repko, “W W Physics at Future Colliders,” *Nucl. Phys. B* **272**, 517 (1986).

- [53] S. Ask, N. D. Christensen, C. Duhr, C. Grojean, S. Hoeche, K. Matchev, O. Mattelaer and S. Mrenna *et al.*, “From Lagrangians to Events: Computer Tutorial at the MC4BSM-2012 Workshop,” arXiv:1209.0297 [hep-ph].
- [54] N. D. Christensen and C. Duhr, “FeynRules - Feynman rules made easy,” Comput. Phys. Commun. **180**, 1614 (2009) [arXiv:0806.4194 [hep-ph]].
- [55] A. Semenov, “LanHEP: A Package for the automatic generation of Feynman rules in field theory. Version 3.0,” Comput. Phys. Commun. **180**, 431 (2009) [arXiv:0805.0555 [hep-ph]].
- [56] T. Stelzer and W. F. Long, “Automatic generation of tree level helicity amplitudes,” Comput. Phys. Commun. **81**, 357 (1994) [hep-ph/9401258].
- [57] J. Alwall, M. Herquet, F. Maltoni, O. Mattelaer and T. Stelzer, “MadGraph 5 : Going Beyond,” JHEP **1106**, 128 (2011) [arXiv:1106.0522 [hep-ph]].
- [58] A. Belyaev, N. D. Christensen and A. Pukhov, “CalcHEP 3.4 for collider physics within and beyond the Standard Model,” arXiv:1207.6082 [hep-ph].
- [59] A. Pukhov, E. Boos, M. Dubinin, V. Edneral, V. Ilyin, D. Kovalenko, A. Kryukov and V. Savrin *et al.*, “CompHEP: A Package for evaluation of Feynman diagrams and integration over multiparticle phase space,” hep-ph/9908288.
- [60] E. Boos, V. Bunichev, M. Dubinin, L. Dudko, V. Edneral, V. Ilyin, A. Kryukov and V. Savrin *et al.*, “CompHEP 4.5 Status Report,” PoS ACAT **08**, 008 (2008) [arXiv:0901.4757 [hep-ph]].
- [61] K. Kong, “TASI 2011: CalcHEP and PYTHIA Tutorials,” arXiv:1208.0035 [hep-ph].
- [62] Computer tutorials at the MC4BSM-2012 workshop, Cornell University, Ithaca NY, March 22-24, 2012, <http://www.phys.ufl.edu/~matchev/mc4bsm6/>.
- [63] J. M. Campbell and R. K. Ellis, “MCFM for the Tevatron and the LHC,” Nucl. Phys. Proc. Suppl. **205-206**, 10 (2010) [arXiv:1007.3492 [hep-ph]].
- [64] C. Williams, “The Matrix Element Method at Next to Leading Order”, talk given at the MC4BSM-6 workshop, Ithaca NY, March 22-24 2012, http://cmssw.cvs.cern.ch/cgi-bin/cmssw.cgi/UserCode/Snowball/MCFM_MatrixElement/README?revision=1.1&view=markup.
- [65] P. Artoisenet and O. Mattelaer, “MadWeight: Automatic event reweighting with matrix elements,” PoS CHARGED **2008**, 025 (2008).
- [66] A. Denner, S. Heinemeyer, I. Puljak, D. Rebuszi and M. Spira, “Standard Model Higgs-Boson Branching Ratios with Uncertainties,” Eur. Phys. J. C **71**, 1753 (2011) [arXiv:1107.5909 [hep-ph]].
- [67] J. Alwall, P. Demin, S. de Visscher, R. Frederix, M. Herquet, F. Maltoni, T. Plehn and D. L. Rainwater *et al.*, “MadGraph/MadEvent v4: The New Web Generation,” JHEP **0709**, 028 (2007) [arXiv:0706.2334 [hep-ph]].
- [68] J. Alwall, P. Artoisenet, S. de Visscher, C. Duhr, R. Frederix, M. Herquet and O. Mattelaer, “New Developments in MadGraph/MadEvent,” AIP Conf. Proc. **1078**, 84 (2009) [arXiv:0809.2410 [hep-ph]].
- [69] N. Tran, “Higgs properties at the LHC”, talk given at the MCTP Higgs Symposium, April 18, 2012, http://www.umich.edu/~mctp/SciPrgPgs/events/2012/higgs/talks/ntran_120418_mctp.pdf.
- [70] The KD_{MAD} code is available at <http://mekd.ihepa.ufl.edu>.

- [71] T. Sjostrand, S. Mrenna and P. Z. Skands, “A Brief Introduction to PYTHIA 8.1,” Comput. Phys. Commun. **178**, 852 (2008) [arXiv:0710.3820 [hep-ph]].
- [72] J. Alwall, A. Freitas and O. Mattelaer, “The Matrix Element Method and QCD Radiation,” Phys. Rev. D **83**, 074010 (2011) [arXiv:1010.2263 [hep-ph]].
- [73] P. Avery, D. Bourilkov, M. Chen, T. Cheng, A. Drozdetskiy, J. S. Gainer, A. Korytov, K. T. Matchev, P. Milenovic, G. Mitselmakher, M. Park, A. Rinkevicius, and M. Snowball, “Improving the Significance of a Higgs Discovery in the Golden Channel $H \rightarrow ZZ^* \rightarrow 4\ell$. Part II. Kinematic discriminants from next-to-leading order matrix elements,” in preparation.